J Neuropathol Exp Neurol
Vol. 75, No. 8, August 2016, pp. 718–730
doi: 10.1093/jnen/nlw044

ORIGINAL ARTICLE

Expression of TRPC6 and BDNF in Cortical Lesions From Patients With Focal Cortical Dysplasia

Da-Hai Zheng, PhD, Wei Guo, PhD, Fei-Ji Sun, MD, Guang-Zhen Xu, MD, Zhen-Le Zang, MS, Hai-Feng Shu, MD, and Hui Yang, MD, PhD

Abstract

Focal cortical dysplasia (FCD) likely results from abnormal migration of neural progenitor cells originating from the subventricular zone. To elucidate the roles in molecules that are involved in neural migration pathway abnormalities in FCDs, we investigated the expression patterns of transient receptor potential canonical channel 6 (TRPC6) and brain-derived neurotrophic factor (BDNF) in cortical lesions from FCD patients and in samples of normal control cortex. TRPC6 and BDNF mRNA and protein levels were increased in FCD lesions. By immunohistochemistry, they were strongly expressed in microcolumns, heterotopic neurons, dysmorphic neurons, and balloon cells (BCs). Colocalization assays revealed that most of the misshapen TRPC6-positive or heterotopic cells had a neuronal lineage with the exception of TRPC6-positive FCDiib patient BCs, which had both neuronal and glial features. Most TRPC6-positive cells were glutamatergic neurons. There was also greater expression of calmodulin-dependent kinase IV (CaMKIV), the downstream factor of TRPC6, in FCD lesions, suggesting that TRPC6 expression promoted dendritic growth and the development of dendritic spines and excitatory synapses via the CaMKIV-CREB pathway in FCD. Thus, overexpression of BDNF and TRPC6 and activation of the TRPC6 signal transduction pathway in cortical lesions of FCD patients may contribute to FC pathogenesis and epileptogenesis.

Key Words: Brain-derived neurotrophic factor; Epilepsy; Focal cortical dysplasia; Malformations of cortical development; Transient receptor potential canonical channel 6.

INTRODUCTION

Focal cortical dysplasia (FCD) is characterized by columnar and laminar disorganization with various cellular abnormalities in the cerebral cortex; it is increasingly recognized as one of the leading causes of medically intractable epilepsy in pediatric patients (1–3). Several cellular and molecular mechanisms underlying the pathogenesis and epileptogenesis of FCD have been proposed, including abnormal migration and maturation of neurons during cortical development and abnormalities of the neuronal circuitry in epileptic foci (4–8). Recent evidence indicates that cells originating from the subventricular zone (SVZ) may be the source of the abnormal cells (eg, dysmorphic neurons ([DNs]) and balloon cells [BCs]) within cortical lesions of patients with FCD (9). In addition, our previous study in a freezing lesions model indicated that SVZ-derived neural progenitors are involved in the formation of focal microgyria (10). However, the mechanisms underlying the abnormal migration of abnormal cells within FCD lesions are not understood.

The transient receptor potential canonical (TRPC) channels are Ca^{2+}-permeable, nonselective cation channels that are expressed in a variety of multicellular organisms (11). Based on their amino acid sequences and functional similarities, the TRPC family can be divided into 3 groups: TRPC1/4/5, TRPC3/6/7, and TRPC2 (11–13). Accumulating evidence indicates that TRPC6 plays a critical role in neuronal development (14–16). For example, in a heteromeric assembly, TRPC6 has an essential role in brain-derived neurotrophic factor (BDNF)-mediated nerve growth cone guidance in conjunction with TRPC3; this suggests that TRPC6 activation may be involved in neuronal migration (16). The development of neuronal circuits requires the establishment of proper neuronal morphology and synapse formation (17). Recent studies have demonstrated that TRPC6 promotes dendritic growth of hippocampal neurons both in culture and in the brain (14). In addition, TRPC6 is localized to both pre- and postsynaptic areas, and TRPC6 overexpression induces excitatory synapse formation (15). Thus, TRPC6 may play a key role in the establishment of neuronal circuits.

In this study, we analyzed surgically resected cortical lesions of FCD patients and postmortem control cortex (CTX) samples to characterize the expression of TRPC6 and BDNF. We found that the expression of TRPC6 and BDNF was increased in the dysplastic cortex compared with the CTX.

From the Department of Neurosurgery, Xinqiao Hospital, Third Military Medical University (D-HZ, F-J, G-ZX, Z-LZ, H-FS, HY), Chongqing, China; Department of Neurosurgery, Tangdu Hospital, Fourth Military Medical University(WG), Xi'an, Shanxi, China; Department of Neurosurgery, General Hospital of Chengdu Military Region(H-FS), Chengdu, Sichuan, China.

Send correspondence to: Hai-Feng Shu, MD, PhD, Department of Neurosurgery, General Hospital of Chengdu Military Region, Chengdu, Sichuan, China; Hui Yang, MD, PhD, Department of Neurosurgery, Xinqiao Hospital, Third Military Medical University, 183 Xinqiao Main Street, Shapingba District, Chongqing 400037, People's Republic of China. E-mail: harvest1979@126.com (H-FS) or huiyang64@yahoo.com (HY).

Da-Hai Zheng and Wei Guo contributed equally to this work.

This work was supported by grants from the National Natural Science Foundation of China (No. 81100975, 81371430).

Supplementary Data can be found at http://www.jnen.oxfordjournals.org.

We also observed greater expression of calmodulin-dependent kinase IV (CaMKIV), the downstream factor of TRPC6, in FCD compared with the CTX.

MATERIALS AND METHODS

Subjects

We examined a total of 44 surgical specimens (18 FCDIa, 14 FCDIIa, and 12 FCDIIb) from patients undergoing surgery for intractable epilepsy. Eight patients had multilobar resections; the remaining 36 patients underwent lesionectomy. All cases were independently reviewed by 2 neuropathologists and the diagnoses were verified based on the FCD grading classification system proposed by the International League Against Epilepsy (18). The patient samples were obtained from the Neurosurgery Department of Xinqiao Hospital at the Third Military Medical University (TMMU), Chongqing, China. All procedures and experiments were conducted under the guidelines approved by the Ethics Committee of the TMMU. All human brain specimens were used in compliance with the Declaration of Helsinki. The clinical characteristics of the FCD patients in this study are summarized in Table 1, and detailed clinical data of the FCD patients are presented in Supplementary Table 1.

For control comparisons, normal-appearing cortex/white matter postmortem samples were obtained from 10 patients (6 male/4 female; mean age: 6.8 years; range: 1.0–12.4 years) who did not have a history of seizures or other neurological diseases, exposure to antiepileptic drugs or evidence of neurological disease at autopsy. All of the autopsies were performed within 6 hours after death. The findings in the control cases were confirmed by 2 neuropathologists. The etiological factors and pathology results of the normal control patients are presented in Table 2.

Tissue Preparation

All resected brain samples were immediately divided into 2 parts at the time of surgery or autopsy. One part was fixed by immersion in 10% buffered formalin for 24 hours and then processed and embedded in paraffin. The paraffin-embedded tissue was sectioned at 7 μm and subjected to histological and immunohistochemical staining. The remaining samples were immediately placed in a cryovial that had been soaked in buffered diethylpyrocarbonate (1:1000) for 24 hours, and then snap frozen in liquid nitrogen. These samples were maintained at −80 °C for subsequent use in real-time polymerase chain reaction (PCR), Western blot, immunofluorescence, and *in situ* hybridization

TABLE 1. Summary of Clinical Characteristics of Patients With FCD

	FCD Ia (n = 18)	FCD IIa (n = 14)	FCD IIb (n = 12)
Male/female	10:8	8:6	7:5
Mean age of surgery (years)	14.6 (range: 2.4–30.8)	6.2 (range: 1.2–12.7)	5.1 (range: 1.1–8.5)
Seizure type	PS (80%); GTCS (42%); Tonic (28%); IS (34%)	PS (59%); GTCS (50%); Tonic (26%); IS (26%)	PS (55%); GTCS (35%); Tonic (22%); IS (25%)
Lesions location	Frontal: 8; Temporal: 10; Parietal: 4; Occipital:3	Frontal: 7; Temporal: 5; Parietal: 4; Occipital: 2	Frontal: 6; Temporal: 4; Parietal: 5; Occipital: 3
Duration of epilepsy (years)	12.4 (range: 1.8–24)	5.5 (range: 1–10.2)	4.2 (range: 1–8)
Seizure frequency (/month)	34 (range: 4–118)	58 (range:10–196)	64 (range: 14–203)
Postoperative outcome (Engel's class)	I: 48%; II: 15%; III: 20%; IV: 17%	I: 59%; II: 20%; III: 11%; IV: 10%	I: 55%; II: 28%; III: 9%; IV: 8%

FCD, focal cortical dysplasia; GTCS, generalized tonic-clonic seizure; IS, infantile spasm; PS, partial seizure.

TABLE 2. Clinical and Neuropathological Characteristics of Control Subjects

Case No.	Sex	Pathology Examination	Age at Surgery (years)	Cause of Death	Brain Region of the Subjects	Application in This Study
1	M	Normal	2.4	Nonneurologic disease	Frontal	Real-time PCR; WB; IHC; ISH
2	M	Normal	6.4	Drowning	Temporal	Real-time PCR; WB; IHC; ISH
3	M	Normal	3.2	Electric shock	Parietal	Real-time PCR; WB; IHC; ISH
4	F	Normal	10.8	Electric shock	Temporal	Real-time PCR; WB; IHC; ISH
5	F	Normal	3.2	Motor vehicle accident	Occipital	Real-time PCR; WB; IHC; ISH
6	M	Normal	1.0	Non-neurologic disease	Frontal; Parietal	Real-time PCR; WB; IHC; ISH
7	M	Normal	3.8	Motor vehicle accident	Frontal; Temporal	Real-time PCR; WB; IHC; ISH
8	M	Normal	3.0	Choking/suffocation	Temporal	Real-time PCR; WB; IHC; ISH
9	F	Normal	6.5	Drowning	Temporal; Occipital	Real-time PCR; WB; IHC; ISH
10	F	Normal	12.4	Motor vehicle accident	Occipital	Real-time PCR; WB; IHC; ISH

M, male; F, Female; IHC, immunohistochemistry (including immunofluorescence); WB, Western blot; Real-time PCR, real-time polymerase chain reaction; ISH, *in situ* hybridization.

analyses. In addition, each frozen sample was stained with hematoxylin and eosin (H&E) to identify the dysplastic sample before it was divided. Finally, all specimens (fixed or frozen) that were used for PCR and Western blotting analyses were carefully inspected by microscopy prior to extraction of messenger RNA and protein using both histological and immunocytochemical staining procedures (H&E, glial fibrillary acidic protein [GFAP], and neuronal nuclear protein [NeuN] immunohistochemical staining) to confirm that the lesion was present in each sample. We also ensured that equal gray/white matter tissue components were available for RNA and protein isolation.

Real-Time PCR Analysis

Real-time quantitative PCR analysis was performed using the RNA prepared from freshly frozen histologically normal human cortex samples (n = 10) and specimens from patients with FCD (FCDI, FCDIIa, FCDIIb; n = 10 in each group). The total RNA from each frozen tissue sample was isolated using TRIzol reagent (Invitrogen, Carlsbad, California). The concentration and purity of the RNA were evaluated by spectrophotometric measurements at 260/280 nm. Single-stranded complementary DNA (cDNA) was synthesized from 1 μg of the total RNA using the ReverTra Ace-α-^{TM} First Strand cDNA Synthesis Kit (Toyobo, Osaka, Japan) in a final volume of 20 μL, according to the manufacturer's protocols. The total mixture was incubated at 42 °C for 90 minutes, heated to 95 °C for 5 minutes, and stored at −20 °C until further use.

PCR primers were designed based on the sequence in NCBI GenBank and synthesized by TaKaRa Bio Inc, Dalian, China. The sequences of the real-time PCR primers are presented in Table 3. For each PCR, all of the procedures were performed on ice. The PCR reaction mixture contained 2 μL of cDNA, 10 μL of SYBR Premix Ex Taq II (TaKaRa), 0.8 μL of both the reverse and forward primers, 0.4 μL of ROX Reference Dye II, and 6 μL of dH_2O (sterile distilled water) for a final volume of 20 μL. Two-step real-time PCR was performed on a 7500 Real-Time PCR System (Applied Biosystems). The cycling conditions were: initial denaturation at 95 °C for 3 minutes, followed by 45 cycles of denaturation at 95 °C for 15 seconds and annealing and elongation at 65 °C for 20 seconds for TRPC6. The annealing and elongation conditions for BDNF were 55 °C for 30 seconds. The data were quantified using 7500 System SDS Software Version 1.2 (Applied Biosystems). Each fluorescent reporter signal was measured against the internal reference dye (ROX) signal to normalize the non-PCR-related fluorescence fluctuations between wells. The relative quantification of each specific product (concentration of each sample divided by the concentration of the reference gene [*β-actin*]) was compared between the patient and control groups.

In Situ Hybridization

In situ hybridization was performed for human TRPC6 using 3 3′ digoxigenin-labeled 19-mer antisense oligonucleotides (TRPC6: 5′ - CGGGG ATCTG ACAAC AGACT GGCTC ACCGG CGGCA - 3′; 5′ - CATCT AAATA GTTTC AATAA TCCTC CAAGA CAATA - 3′; 5′ - TTATC CATGG AACCA AATCA AGAGG AAACC AATAG - 3′). The oligonucleotides (synthesized by Boster, Wuhan, China) were hybridized to 7-μm sections of paraffin-embedded FCD specimens at 42 °C, as previously described (19). To detect the hybridization signals, we used a biotinylated mouse antidigoxin antibody (AR0147, Boster) and a horseradish peroxidase-conjugated goat anti-mouse polyclonal antibody (AR0149, Boster) as the secondary antibody; the sections were developed with diaminobenzidine (DAB, Boster). Several negative controls were conducted using a nonsense probe or omitting the specific probe for TRPC6.

Western Blot Analysis

Western blot analysis was performed to quantify the levels of the BDNF, TRPC6, and CaMKIV proteins in homogenates from FCDI cortical lesions (n = 10), FCDIIa cortical lesions (n = 10), FCDIIb cortical lesions (n = 10), and CTX samples (n = 10). Glyceraldehyde 3-phosphate dehydrogenase (GAPDH) was evaluated as a loading control. Freshly frozen CTX and FCD specimens were dissected as previously described and homogenized in a lysis buffer containing 10 mmol/L Tris (pH 8.0), 150 mmol/L NaCl, 10% glycerol, 1% NP-40, 0.4 mg/mL Na-orthovanadate, 5 mmol/L EDTA (ethylenediaminetetraacetic acid, pH 8.0), 5 mmol/L NaF, and 10% protease inhibitor cocktail (Sigma, St. Louis, Missouri) (19). The protein concentration was estimated using the Bradford method (Bio-Rad, Richmond, California), with bovine serum albumin (BSA) as the standard. Equal quantities of protein (50 μg/lane) were electrophoresed on 8%, 10%, or 15% sodium dodecyl sulfate–polyacrylamide gels, according to the size of the target proteins. The proteins were subsequently transferred onto polyvinylidene fluoride membranes (Millipore, Billerica, Massachusetts) using a wet electroblotting system (Transblot SD; Bio-Rad). After blocking for 1 hour in TBST (20 mmol/L Tris, 150 mmol/L NaCl, and 1% Tween, pH 7.5) with 5% nonfat dry milk, the membranes were incubated with one of the following primary antibodies overnight at 4 °C: GAPDH (mouse monoclonal, 1:1000; Chemicon, Temecula, California); BDNF (rabbit polyclonal, 1:1000; Santa Cruz Biotechnology, Santa Cruz, California); TRPC6 (rabbit polyclonal, 1:500; Sigma); and CaMKIV (rabbit polyclonal, 1:500; Sigma). The blots were then treated with a horseradish peroxidase-conjugated goat anti-rabbit or goat anti-mouse

TABLE 3. Primer Characteristics

	Sense Primer (5′→3′)	Antisense Primer (5′→3′)
BDNF	TCAATGGAAGAGGCCAGGACAGA	GAACAGACAGGATGGGCAGAAGG
TRPC6	CCGCTGCCTTGCTACGGCTACT	TCTTCCGCACCACTGGGATGTT
β-actin	AGCGAGCATCCCCCAAAGTT	GGGCACGAAGGCTCATCATT

secondary antibody (1:3000; Santa Cruz Biotechnology) for 1 hour at room temperature after several TBST washes. Enhanced chemiluminescence was used to detect the signal.

Negative controls were performed to characterize the specificity of the primary antibodies for BDNF, TRPC6, and CaMKIV. Preadsorbing the BDNF, TRPC6, and CaMKIV antibodies against their corresponding antigens prior to the Western blot procedure resulted in complete blockage of specific signals.

Histological, Immunohistochemical, and Double-Immunofluorescence Staining

The sections prepared above were routinely stained with H&E and consecutive serial sections were used for the immunohistochemical studies. For single-label immunohistochemistry, sections were deparaffinized in xylene (10 minutes), rehydrated with a graded alcohol series, and then incubated for 30 minutes in 0.3% H_2O_2 diluted in methanol to quench endogenous peroxidase activity. Antigen retrieval was performed by heating the sections in phosphate buffer (0.01 mol/L, pH 7.3) for 20 minutes using a microwave oven. The sections were washed with phosphate-buffered saline (PBS) and incubated in 10% normal goat serum for 60 minutes at room temperature, followed by overnight incubation with anti-TRPC6 (rabbit polyclonal, 1:100; Sigma) or anti-BDNF (rabbit polyclonal, 1:500; Santa Cruz Biotechnology), primary antibodies at 4 °C. On the following day, after 3 rinses with PBS, the sections were incubated with goat anti-rabbit immunoglobulins conjugated to a peroxidase labeled-dextran polymer (EnVision+ System-HRP, Boster) for 60 minutes at 37 °C. The immunoreactions were visualized with 3,3′ diaminobenzidine tetrahydrochloride (Boster). The sections were counterstained with hematoxylin. To evaluate the specificity of the staining, some sections were immunostained by preabsorbing the polyclonal antibodies using excess antigen as a negative control (20, 21). All staining was abolished in the negative control experiments. A Leica DMIRB microscope (Leica, Nussloch, Germany) was used to acquire the images.

For double-immunofluorescence staining, paraffin-embedded sections were incubated with primary anti-TRPC6 antibody (rabbit polyclonal, 1:100; Sigma) combined with anti-NeuN (mouse monoclonal, 1:100; Millipore), anti-GFAP (mouse monoclonal, 1:500; Sigma), anti-HLA-DP, DQ, DR (mouse monoclonal, 1:100, Dako, Glostrup, Denmark), anti-glutamate (mouse monoclonal, 1:1500; Sigma), anti-GABA (mouse monoclonal, 1:500; Sigma), anti-GAD65 (mouse monoclonal, 1:500; Sigma), or anti-GAD67 (mouse monoclonal, 1:500; Sigma) antibodies in 0.01 M PBS (pH 7.4) containing 1% BSA overnight at 4 °C. After 3 rinses with PBS, the sections were incubated with a mixture of fluorescein isothiocyanate (FITC)-conjugated goat anti-rabbit IgG (1:300; Southern Biotechnology Associates, Inc., Birmingham, Alabama) and AlexaFluor 594-conjugated goat anti-mouse IgG (1:500; Invitrogen) secondary antibodies for 1 hour at 37 °C. Vectashield containing DAPI ([4',6-diamidino-2-phenylindole] 10 kg/mL, Beyotime, Beijing, China) was used to label the DNA in cell nuclei by incubating the sections for 15 minutes at 37 °C. Next, after 3 washes, the slides were coverslipped with 50% glycerol in 0.1 M PBS. The fluorescent sections were observed and photographed with a confocal laser-scanning microscope (TCS-TIV; Leica).

Several controls were performed for characterization of the specificity of the primary anti-TRPC6 antibody. To ensure that the primary antibodies did not cross-react with unrelated secondary antibodies in double-immunofluorescent staining experiments, some sections were incubated with FITC-conjugated goat anti-rabbit IgG (1:300; Southern Biotechnology Associates, Inc.) after incubation with mouse neuronal markers or with AlexaFluor 594-conjugated goat anti-mouse immunoglobulin G (1:500; Invitrogen) after incubation with the anti-TPRC6 antibody (rabbit polyclonal, 1:100; Sigma). Further confirmation of the specificity of TRPC6 was conducted by preabsorbing the antibody with its corresponding antigen prior to double immunofluorescence staining.

Western Blot Analysis

Western blots were densitometrically analyzed using Image-Pro Plus software (Media Cybernetics, Silver Spring, Maryland). The optical density (OD value) of each protein band was calculated relative to the OD value of the reference protein GAPDH.

Evaluation of Immunostaining and Cell Counting

All labeled tissue sections were evaluated by 2 independent observers who were blind to the identification codes of the samples. The observers evaluated the specific immunostaining results to determine the presence or absence of various histopathological parameters, identify specific immunoreactivity for the different markers and to count the cells. The overall concordance was greater than 85%, and the overall kappa value ranged from 0.86 to 0.95. In cases where the observers disagreed, both observers performed independent re-evaluations to determine the final score.

For the IHC experiments, we stained 3 representative sections per case with the anti-TRPC6 and -BDNF antibodies. Each section that was used to examine BDNF and TRPC6 immunoreactivity with a Leica microscope was divided into 200 high-power nonoverlapping fields using a square grid inserted into the eyepiece (0.0625×0.0625 mm width, corresponding to 781.250 μm^2). The staining intensity was evaluated with a semiquantitative scale ranging from 0 to 3 (0: −, absent; 1: +, weak staining; 2: ++, moderate staining; 3: +++, strong staining). The intensity scores are presented in Table 4. This score represents the predominant staining intensity of the

TABLE 4. Intensity Score of TRPC6 and BDNF-Immunopositive Cells in Control and FCD Specimens

	CTX (n = 10)	FCDIa (n = 18)	FCDIIa (n = 14)	FCDIIb (n = 12)
BDNF	0.36 ± 0.19	1.58 ± 0.47**	2.06 ± 0.53**#	2.23 ± 0.49**#
TRPC6	0.89 ± 0.35	1.63 ± 0.58*	2.28 ± 0.31**#	2.34 ± 0.23**#

FCD, focal cortical dysplasia; Data are expressed as mean ± SE.
*p < 0.05; **p < 0.01; (FCD vs CTX, by one-way ANOVA); #p < 0.05 (FCDIIa, IIb vs FCDIa, by one-way ANOVA).

cells in each section and was calculated as the average of the selected fields.

In addition, the numbers of TRPC6- and BDNF-immunoreactive BCs/DNs in the FCD cases were quantified, as previously described (19). H&E staining usually enables misshapen cells, such as DNs and BCs, to be distinguished clearly from other cell components based on their characteristic cytological properties. DNs exhibit a significantly enlarged cell body and nucleus, aggregations of Nissl substance toward the cell membrane, and accumulated phosphorylated and unphosphorylated neurofilament isoforms in the cytoplasm, whereas BCs have eccentric nuclei, a ballooned cytoplasm, and do not exhibit clear axonal or dendritic processes. Only cells that exhibited these distinct cytological properties were included in the analysis. The sections were selected at 35-μm intervals, and the mean area for the quantitative analysis was 5.95 mm^2. All BCs/DNs within this region were systematically counted at high magnification (×40 objective) and described as positive (including strong or intermediate immunoreactivity) or negative. The percentage of labeled BCs (or DNs) was calculated based on the total number of BCs (or DNs). For each case, 3 sections in each paraffin block were averaged; this average value was used for the statistical analysis.

Data Analysis and Statistics

Data are expressed as mean ± SE. Statistical analyses were performed with Statistical Package for the Social Sciences for Windows (SPSS 13.0, SPSS Inc., Chicago, IL). Differences between the experimental groups were analyzed by one-way ANOVA (analysis of variance); $p < 0.05$ was considered significant.

RESULTS

Expression of TRPC6 mRNA in Cortical Lesions of FCD Patients

We first studied the expression of TRPC6 mRNA in FCD patients by quantitative PCR. Greater TRPC6 mRNA levels were observed in the FCDIa, FCDIIa, and FCDIIb groups compared with the CTX samples (Fig. 1A). Importantly, the mRNA expression levels were significantly higher in the FCDIIa and FCDIIb cortical lesions than in the FCDIa specimens (Fig. 1A). Additionally, we performed *in situ* hybridization to study the cellular distribution of TRPC6 mRNA in the FCD cases. In the control samples, TRPC6 mRNA was weakly distributed in neurons and cells with a glia-like morphology (Fig. 1B–D). TRPC6 mRNA was widely distributed in neurons and glia-like cells in the FCD tissues (Fig. 1E–I), particularly in the microcolumns, heterotopic neurons, DNs, and BCs (Fig. 1E–I). No positive signal was observed in sections treated with a nonsense probe or without the addition of the specific probe for TRPC6 (data not shown).

Expression of TRPC6 Protein in Cortical Lesions From FCD Patients

To confirm the upregulation of TRPC6 in FCD patients, we assessed TRPC6 protein levels by Western blot. TRPC6 was present as a band of approximately 106 KDa. Increased levels of TRPC6 protein were observed in the FCDIa, FCDIIa, and FCDIIb groups compared with the control samples (Fig. 2A). TRPC6 protein levels were significantly higher in the FCDIa, FCDIIa, and FCDIIb tissues than in the control samples. Moreover, TRPC6 protein levels were significantly greater in the FCDIIa and FCDIIb cortical lesions compared with the FCDIa specimens (Fig. 2B). In the absorption control, no band was detected at the corresponding position (data not shown).

Immunohistochemistry and Double Immunofluorescence

In the human control cortical autopsy specimens there was weak to moderate TRPC6 staining detected in the cell bodies and dendrites of neurons throughout the cortical layers (Fig. 3A, B); concurrently, weak to moderate staining was detected in the glia-like cells in the white matter and junction (Fig. 3B, C). Double-labeling experiments confirmed that TRPC6 was expressed in NeuN-positive neurons (Fig. 3B, inset), including glutamatergic (Fig. 3E–G) and GABAergic neurons (Fig. 3H–J), and was also expressed in GFAP-positive astrocytes (Fig. 3D).

In the FCDIa cortical lesions there was moderate to strong TRPC6 immunostaining in the neurons (Fig. 3K–O), including the microcolumns, pyramidal neurons, and heterotopic neurons in the white matter. In addition, moderate to strong TRPC6 staining was detected in the glia-like cells in the white matter and junction (Fig. 3L, M). The intensity of TRPC6 immunoreactivity in the FCDIa cortical lesions was significantly higher than that in the control samples (Table 4). The double-labeling experiments demonstrated that TRPC6 was expressed in NeuN-positive neurons (Fig. 3N,O, insets), most of which were glutamatergic neurons (Fig. 3Q) and a few were GABAergic neurons (Fig. 3Q–T). Intriguingly, TRPC6 was coexpressed with glutamate in the microcolumns (Fig. 3K inset) and heterotopic neurons (Fig. 3M, inset), but almost no TRPC6-positive microcolumns or heterotopic neurons expressed markers of GABAergic neurons, GABA, GAD65, and GAD67, suggesting that they were glutamatergic neurons. In addition, TRPC6 colocalized with several GFAP-positive astrocytes (Fig. 3P) but not with HLA-positive microglia (not shown).

In the FCDIIa samples, moderate to strong TRPC6 staining was detected in 74% ± 4.3% of the DNs (n = 896) (Fig. 4A–C), of which 52% ± 4.3% exhibited strong staining (Fig. 4B, C). Strong staining was also displayed in cells exhibiting glial morphology (Fig. 4B). The intensity scores revealed prominent upregulation of TRPC6-immunoreactivity (-IR) in the FCDIIa specimens compared with the control samples and FCDIa tissues (Table 4). Double-labeling experiments revealed that most of the TRPC6-positive DNs coexpressed the neuronal marker NeuN (Fig. 4C inset, 4D). Most of these neurons were excitatory neurons (colabeled with glutamate) (Fig. 4H), and a few were inhibitory neurons (GAD65-, GAD67- and GABA-positive) (Fig. 4I–K). Coexpression of TRPC6 and GFAP was observed in some astrocytes (Fig. 4E–G), but almost none of the TRPC6-positive cells expressed the microglial marker HLA-DR (not shown).

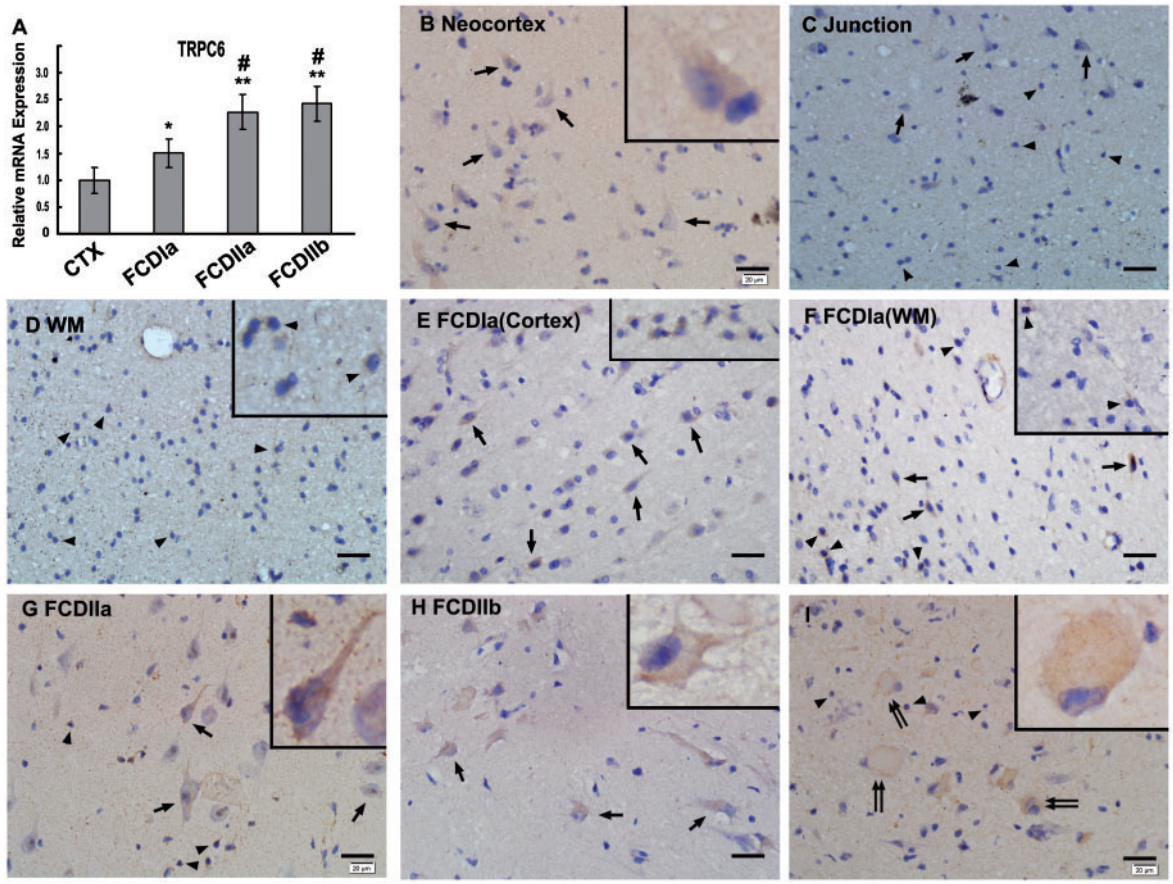

FIGURE 1. Expression of TRPC6 mRNA in CTX and in patients with FCD types Ia, IIa, and IIb. **(A)** Real-time polymerase chain reaction analysis of TRPC6 mRNA expression in CTX, FCDIa, FCDIIa, and FCDIIb (n = 10/group) specimens. Increased TRPC6 mRNA levels were observed in the FCDIa, FCDIIa, and FCDIIb samples versus CTX samples. Importantly, the expression of TRPC6 mRNA was significantly increased in the FCDIIa and FCDIIb cortical lesions compared with the FCDIa specimens. Error bars represent SE; *$p < 0.05$, **$p < 0.01$ versus CTX; #$p < 0.05$ versus FCDIa; ANOVA. **(B–I)** *In situ* hybridization analysis of TRPC6 mRNA expression. TRPC6 mRNA expression in CTX samples **(B–D)**. Expression was observed in neurons (arrows in **B** and **C**) and glia-like cells (arrowheads in **C** and **D**) in the neocortex, white matter (WM), and junction. TRPC6 mRNA expression in FCDIa samples **(E, F)**. Expression was observed in neurons (arrows in **E**), including microcolumns (insert in **E**), heterotopic neurons (arrows in **F**) in the white matter, and glia-like cells (arrowheads in **F**). TRPC6 mRNA expression in FCDIIa samples **(G)**. Expression was observed in dysmorphic neurons (DNs, arrows in **G**) and glia-like cells (arrowheads in **G**). TRPC6 mRNA expression in FCDIIb samples **(H, I)**. Expression was observed in dysmorphic neurons (DNs, arrows in **H** and inset), balloon cells (BCs, double-arrows in **I**), and glia-like cells (arrowheads in **I** and inset). Scale bar: 30 μm.

In the FCDIIb cases, moderate to strong TRPC6 staining was detected in 76% ± 5.7% of the DNs (n = 852) (Fig. 4L–N) and 68% ± 4.9% of the BCs (n = 497) (Fig. 4L, M, O), along with moderate to strong expression in the glial cells (Fig. 4M). The intensity scores indicated that TRPC6-IR was significantly increased in the FCDIIb specimens compared with the control samples and FCDIa tissues. There was no significant difference between the FCDIIa and FCDIIb specimens (Table 4).

Double labeling demonstrated that TRPC6 was coexpressed with the neural marker NeuN in the neurons, including the DNs (insert in Fig. 4N) and BCs (insert a in Fig. 4O); most were glutamate-positive (Fig. 4P), suggesting that they were excitatory neurons. In addition, some of the TRPC6-positive neurons coexpressed GABA (Fig. 4Q), GAD65 (Fig. 4R), and GAD67 (Fig. 4S), indicating they were inhibitory neurons. Moreover, TRPC6 staining was also detected in several GFAP-positive astrocytes (Fig. 4U–W). Interestingly, TRPC6-positive BCs coexpressed both neuronal and astrocytic markers (insert b in Fig. 4O), suggesting that BCs are of both neural and glial lineages. None of the TRPC6-positive cells expressed the microglia marker HLA-DR (Fig. 4T).

In immunochemistry experiments, no staining for TRPC6 appeared in the preabsorption control (data not shown). No cross-reactivity was observed between the rabbit-raised primary antibody and the anti-mouse secondary antibody or, vice versa, in double-labeling experiments (data not shown). No reactive products of TRPC6 appeared in the preabsorption control in double-labeling experiments (data not shown).

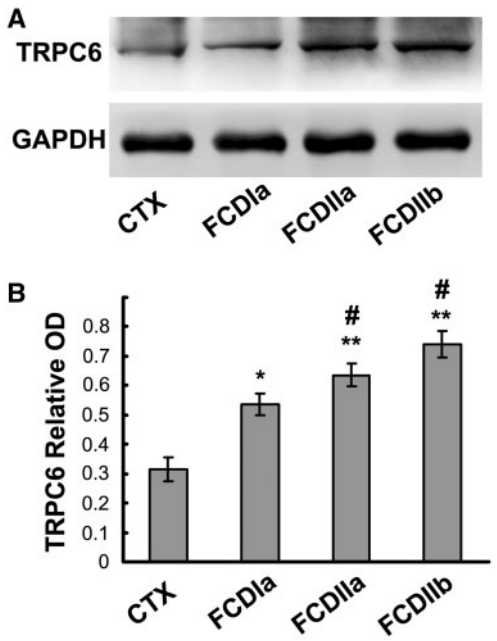

FIGURE 2. Expression of TRPC6 protein in CTX and FCD types Ia, IIa, and IIb. **(A)** Representative immunoblot of TRPC6 in total homogenates of lesions from FCD types Ia (FCDIa), IIa (FCDIIa), and IIb (FCDIIb) (n = 10 in each series) and the control CTX tissues (n = 10). **(B)** Densitometric analyses of the Western blots. There was a significant increase in TRPC6 protein levels in the FCDIa, FCDIIa, and FCDIIb tissues versus control samples. The TRPC6 protein levels were also significantly greater in the FCDIIa and FCDIIb cortical lesions versus the FCDIa specimens. Error bars represent SE; *$p < 0.05$, **$p < 0.01$ versus CTX; #$p < 0.05$ versus FCDIa; ANOVA.

Expression of BDNF mRNA in Cortical Lesions of FCD Patients

The expression of BDNF mRNA was evaluated by quantitative PCR in the FCD and CTX tissues; on average, a 1.5- to 2.5-fold increase was observed in the FCDIa, FCDIIa, and FCDIIb samples compared with the control cortex. BDNF mRNA levels were significantly increased in the FCDIIa and FCIIb tissues compared with the FCDIa tissues. There were no significant differences between FCDIIa and FCDIIb (Fig. 5A).

Western Blot Analysis of BDNF

In the Western blot analysis of the tissue homogenates, BDNF was present as a band of approximately 17 KDa (Fig. 5B). There was a significant increase in BDNF protein levels in the total homogenates from the FCDIa, FCDIIa, and FCDIIb cases compared with the CTX. BDNF protein expression levels were significantly increased in the FCDIIa and FCDIIb cortical lesions compared with the FCDIa specimens. There was no significant difference between the expression of BDNF in the FCDIIa and FCDIIb specimens (Fig. 5C). In the absorption control, no band was detected at the corresponding position (data not shown).

Cellular Distribution of BDNF in the Cortical Lesions of FCD Patients

Weak to moderate BDNF staining was detected in neurons throughout the cortical layers and in glia-like cells in the white matter of CTX specimens (Fig. 5D–F).

In FCDIa cortical lesions, moderate to strong BDNF staining was observed in the neurons, including the microcolumns in the gray matter (Fig. 5G) and heterotopic neurons in the white matter (Fig. 5H). There was also moderate BDNF staining in glia-like cells (Fig. 5H). The intensity scores indicated that BDNF-IR was higher in the FCDIa samples than in the control cortex (Table 4).

In the FCDIIa samples, moderate to strong BDNF expression was detected in 88% ± 5.6% of the DNs (n = 857); of these, 57% ± 3.8% expressed strong staining (Fig. 5I, J). As in the FCDIa specimens, moderate to strong staining was observed in glial cells (insert in Fig. 5J). The intensity scores revealed that BDNF-IR was increased in the FCDIIa specimens compared with the CTX samples and FCDIa tissues (Table 4).

In the FCDIIb cases, there was moderate to strong BDNF-IR in 83% ± 4.1% of the DNs (n = 834, Fig. 5K,L), and 72% ± 4.5% of the BCs (n = 415, Fig. 5K,L), along with moderate to strong staining in the glia-like cells (Fig. 5K,L). The intensity scores confirmed that BDNF-IR was significantly increased in the FCDIIb specimens compared with the control samples and FCDIa tissues but there was no significant difference between the FCDIIa and FCDIIb specimens (Table 4). No staining for BDNF appeared in the preabsorption control (data not shown).

Expression of CaMKIV in Cortical Lesions of FCD

CaMKIV expression was increased in the cortical lesions of the FCDIa, FCDIIa, and FCDIIb cases compared with the CTX cases by Western blotting. The protein detected by immunoblotting was a band of 65 KDa. The CaMKIV bands in the FCDIa, FCDIIa, and FCDIIb samples were more intense than those from the CTX samples (Fig. 6A). CaMKIV protein levels were significantly increased in the FCDIa, FCDIIa, and FCDIIb samples compared with the CTX samples. Importantly, the CaMKIV protein levels were greater in the FCDIIa and FCDIIb samples versus the FCDIa samples (Fig. 6B). No band was detected at the corresponding position in the absorption control (data not shown).

DISCUSSION

Transient receptor potential (TRP) channels are crucial nonselective ion channel components of neurons, epithelial, blood, and smooth muscle cells; thus, they are important targets for treating diseases that arise from the dysfunction of these channels (22). A recent study confirmed that the expression of TRPV1, a TRP channel, is increased in the cortex and hippocampus of patients with mesial temporal lobe epilepsy (23). Shu et al (24) also confirmed that TRPV1 was increased in the cortical lesions of TSC and FCDIIb samples compared with the normal control cortex, suggesting the possible involvement of TRPV1 in the intrinsic and increased epileptogenicity in epilepsy that results from malformations of cortical

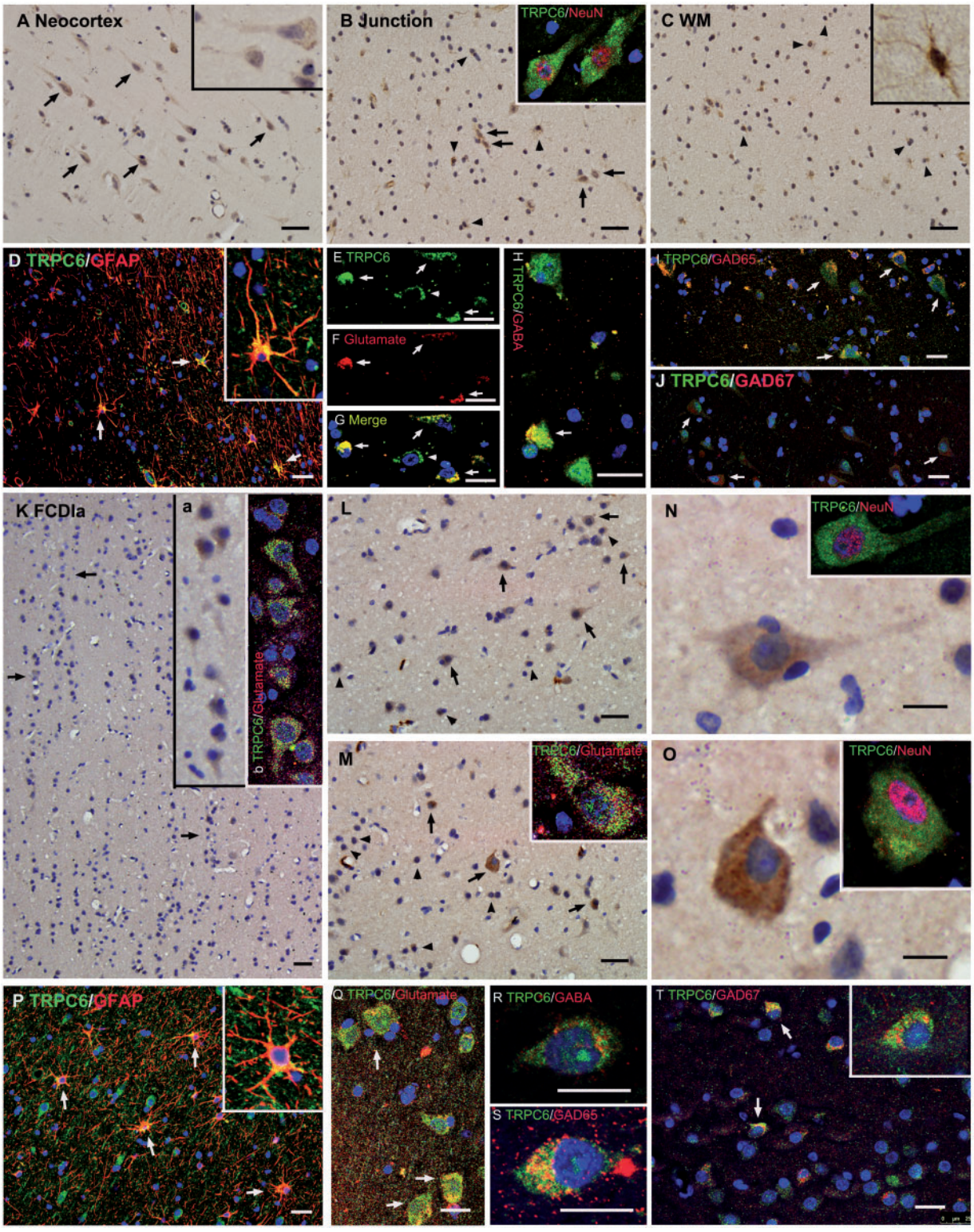

FIGURE 3. Cell-specific distribution of TRPC6 in CTX and FCDIa samples. **(A–C)** TRPC6 in the normal control cortex (CTX). Representative photomicrographs of immunohistochemical staining for TRPC6 in the control cortex **(A)**, junction **(B),** and white matter (WM) **(C)**, showing weak to moderate TRPC6 staining in neurons (arrows in **A** and **B**) and glia-like cells (arrowheads in **B** and **C**). **(B inset, D–J)** Double-label immunofluorescence showing TRPC6-positive cells in the control cortex. TRPC6 is shown in green; nuclei are stained with DAPI (blue). Antibodies against NeuN (**B**, inset) and glial fibrillary acidic protein (GFAP) **(D)** were used to label neurons and astrocytes, respectively. Antibodies against glutamate, glutamic acid decarboxylase 65 (GAD65),

development. Tai et al (25) also reported that TRPC5 channels may play an important role in the generation of prolonged neuronal depolarization and bursting during the epileptiform seizure discharges of epilepsy. Phelan et al (26) first identified a functional role for TRPC7 in the initiation of seizures both *in vitro* and *in vivo*. Here, we demonstrated that TRPC6 and its downstream signaling factor CaMKIV are upregulated in brain tissues from patients with FCD compared with controls. TRPC6 was expressed at characteristically high levels in neuronal microcolumns, heterotopic neurons, DNs, and BCs. In addition, BDNF, which is the potential guidance cue that directs nerve growth cones via TRPC6 (16), was also expressed at high levels in the cortical lesions of FCD patients and was generally located in reactive astrocytes, neuronal microcolumns, heterotopic neurons, DNs, and BCs. Taken together, these data suggest that BDNF may contribute to the pathogenesis of heterotopic cells within epileptic foci via the TRPC6 pathway and may play an important role in the epileptogenesis of FCD. However, the mechanistic details require additional functional investigations.

It has been reported that the expression of TRPC6 in rat hippocampus peaks between postnatal days 7 and 14 (14), and that TRPC6 is present in the postsynaptic sites of hippocampal neurons (15). In this study, we found that the TRPC6 mRNA and protein levels were significantly higher in FCD lesions than in the control CTX tissues, suggesting that TRPC6 may be involved in the pathogenesis of the cortical lesions of FCD.

TRPC6 has been identified in many rodent brain regions and is preferentially expressed in Purkinje cells and neurons of the basal ganglia (27). In this study, immunofluorescence experiments further confirmed that TRPC6 is expressed in NeuN-positive neurons and sporadic GFAP-positive astrocytes but not in HLA-DR-positive microglia in the CTX and FCD tissues; this suggests that TRPC6 is expressed in cells of a neuronal lineage and in a few cells of a glial lineage. In FCD samples, most of the TRPC6-positive neurons were glutamatergic neurons, and a few were GABAergic neurons. However, in CTX tissues, there was no obvious difference in the numbers of glutamatergic and GABAergic neurons, raising the possibility that the TRPC6-positive neurons in FCD patients may be hyperexcitable. We also confirmed that the neurons in the microcolumns and the heterotopic neurons were glutamatergic. In FCD samples, TRPC6 colocalized with glutamate and GABA in the DNs and BCs, which indicated that they were glutamatergic or GABAergic neurons. GABAergic neurons are distributed in layers II and III in the neocortex of certain areas of the human brain, such as sensory and motor areas, temporal and frontal association areas, and paralimbic regions (28, 29). This study suggests that activation of TRPC6 might induce disruption of the excitatory/inhibitory balance in the epileptic zone of FCD patients.

It has been widely accepted that FCD results from abnormal migration, resulting in heterotopic white matter neurons, disorganized lamination, and abnormalities in maturation and differentiation (6, 7, 30); DNs and BCs in FCD may be derived from the proliferative regions of SVZ (9). A previous study showed that TRPC6, in conjunction with C3 in a heteromeric assembly, plays an essential role in the BDNF-mediated guidance of nerve growth cones (16, 31, 32). Our data demonstrate that the expression of BDNF was increased in FCD patients and specifically distributed in heterotopic white matter neurons, DNs, and BCs, suggesting that the BDNF/TRPC6 pathway may be involved in the formation of heterotopic neurons, DNs, and BCs by guiding nerve growth cones. Because of the limitations of the descriptive experiments performed here, further investigations of migration in animal models of FCD are required to support this hypothesis.

In this study, we observed that BDNF and TRPC6 were specifically distributed in DNs and BCs. It has been reported that DNs can spontaneously produce "epileptic-like" activity (33), suggesting that these cytomegalic cells are likely the "epileptic neurons" in FCD. Mathern et al (8) suggested that DNs and BCs might result from a partial failure of programmed cell death during postcorticoneurogenesis in the remnants of the molecular layer and that seizure generation in FCD patients is the consequence of incomplete cerebral development, with abnormal interactions between immature and mature cells, and cellular networks. BDNF is a potent target-derived prosurvival protein that supports the viability of both peripheral and central neurons (34–37); the BDNF-induced survival mechanism relies on convergent Ca^{2+}-dependent signaling pathways (38). The binding of BDNF to TrkB results in the

FIGURE 3. Continued
glutamic acid decarboxylase 67 (GAD67), and γ-aminobutyric acid (GABA) were used to label glutamatergic neurons and GABAergic neurons and are also shown in red **(E–J)**. The merged images are shown in yellow. The merged images show the colocalization of TRPC6 (green) with NeuN (red) in neurons (**B**, insert) and with GFAP (red) in astrocytes (arrows in **D** and inset). TRPC6 (green, **E**) was coexpressed with the excitatory neurotransmitter glutamate (red, **F**) in neurons of the CTX samples (arrows in **E–G**), suggesting that they are glutamatergic neurons. Merged images show that TRPC6 (green) is coexpressed with the inhibitory neurotransmitter GABA (red) (arrows in **H**), and with GAD65 and GAD67 (red) in neurons of the CTX samples (arrows in **I** and **J**), indicating that they are GABAergic neurons. **(K–T)** TRPC6 in focal cortical dysplasia (FCD) type Ia (FCDIa) samples. Representative photomicrographs of immunohistochemical staining for TRPC6 in the cortex **(K)**, junction **(L)**, and white matter **(M)** of FCDIa samples, showing moderate to strong TRPC6 staining in neurons (arrows in **K–O**), including the microcolumns (insert a in **K**), pyramidal neurons **(N)** and heterotopic neurons (arrows in **M** and **O**) in the white matter, and glia-like cells (arrowheads in **L** and **M**). (Insert b in **K**, **M–T**) Merged images show the colocalization of TRPC6 (green) and NeuN (red) in the pyramidal neurons (insert in **N**) and heterotopic neurons (insert in **O**) and the colocalization with GFAP (red) in astrocytes **(P)**. Double-label immunofluorescence confirmed that the neurons in the microcolumns (insert b in **K**) and the heterotopic neurons (insert in **M**) are glutamatergic neurons. The merged images also show the colocalization of TRPC6 (green) with the marker of glutamatergic neurons, glutamate (red) (arrows in **Q**), and with the markers of GABAergic neurons, GABA (red) **(R)**, GAD65 (red) **(S)**, and GAD67 (red) (arrows in **T**), in neurons of the FCDIa samples. Scale bars: **A–C, K–M** = 30 μm; **D–J, P, Q, T** = 25 μm; **N, O, R, S** = 10 μm.

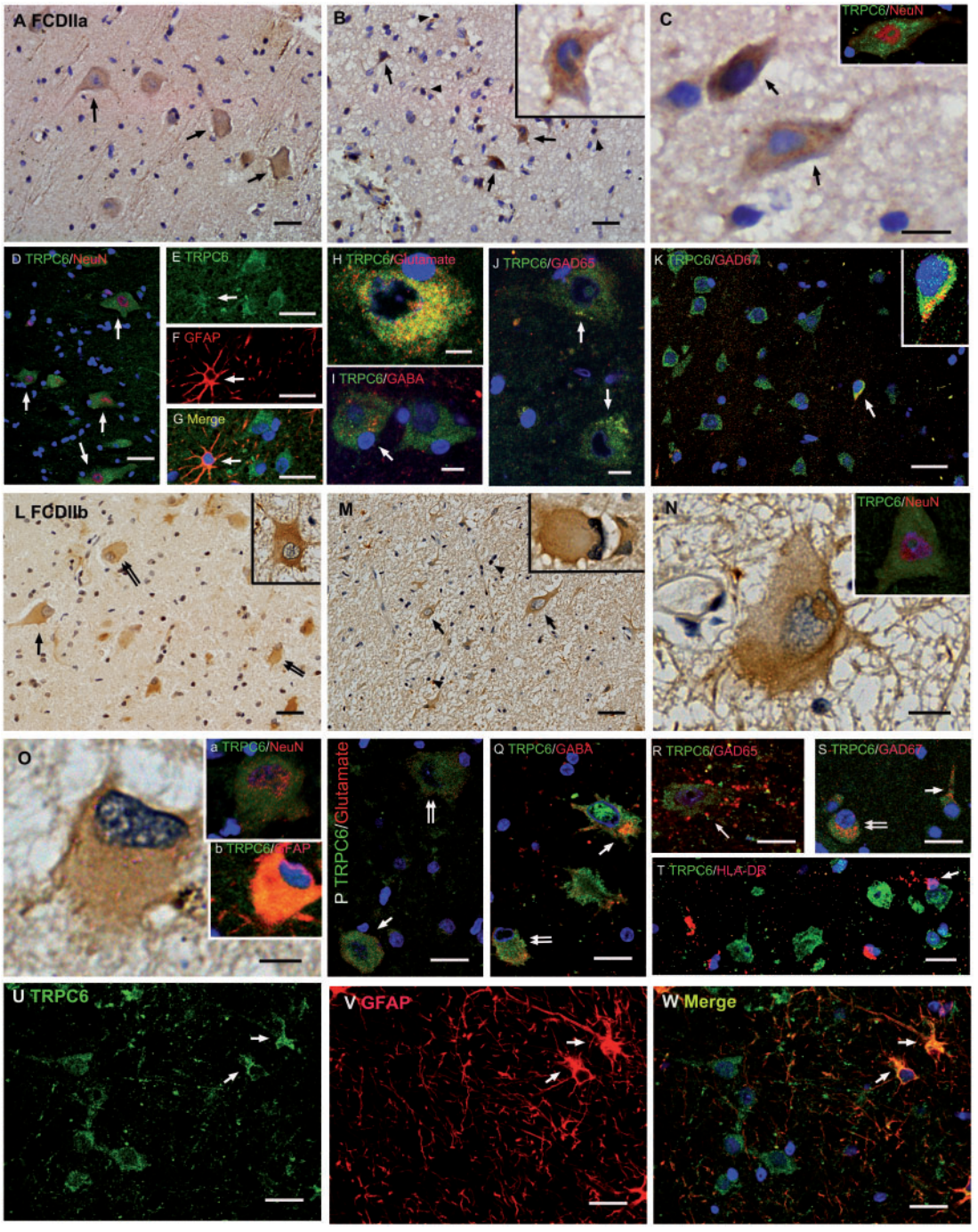

FIGURE 4. Cell-specific distribution of TRPC6 in FCD types IIa and IIb. **(A–K)** TRPC6 in focal cortical dysplasia (FCD) type IIa (FCDIIa) samples. **(A–C)** There is moderate to strong TRPC6-immunoreactivity (-IR) in neurons, particularly the dysmorphic neurons (DNs), throughout the cortical layers (arrows in **A** and **C**) and in the white matter (arrows in **B**). Moderate to strong TRPC6-IR was also observed in glia-like cells in the FCDIIa samples (arrowheads in **B**). (Inset in **C, D–K**) Merged images show the colocalization of TRPC6 (green) with NeuN (red) (inset in **C, D**) in the DNs. Some scattered reactive astrocytes (GFAP-positive) are colabeled with TRPC6 (arrows in **E–G**). Double-label immunofluorescence shows that the TRPC6-positive DNs coexpressed either glutamate **(H)** or GABA (arrows in **I**); a few TRPC6-positive neurons colocalized with GAD65 (arrows in **J**) and GAD67 (arrows in **K**). **(L–W)** TRPC6 in FCD type IIb (FCDIIb) samples. There is moderate to strong TRPC6-IR in neurons, including dysmorphic neurons (DNs, arrows in **L–N**) and balloon cells (BCs, double-arrows in **L** and **O**). There is also moderate to strong TRPC6-IR in glia-like cells in the FCDIIb samples (arrowheads in **M**). **(N–W)** Merged images show colocalization of TRPC6 (green) with NeuN (red) (insert in **N**) in dystrophic neurons (DNs). TRPC6-positive BCs coexpress NeuN (insert in **O**) and glutamate (arrows in **P**). Double-label immunofluorescence showed that most of the TRPC6-positive BCs (double arrows) coexpressed glutamate **(P)**. A few TRPC6-positive DNs and BCs coexpressed GABA, GAD65, and GAD67 (arrows in **Q, R, S**). TRPC6 was localized to a few GFAP-positive astrocytes (arrows in **U–W**) but not HLA-positive microglia (arrows in **T**). Scale bars: **A, B, D–G, K–M** = 30 μm; **C, N, H–J, O** = 10 μm; **P–W** = 20 μm.

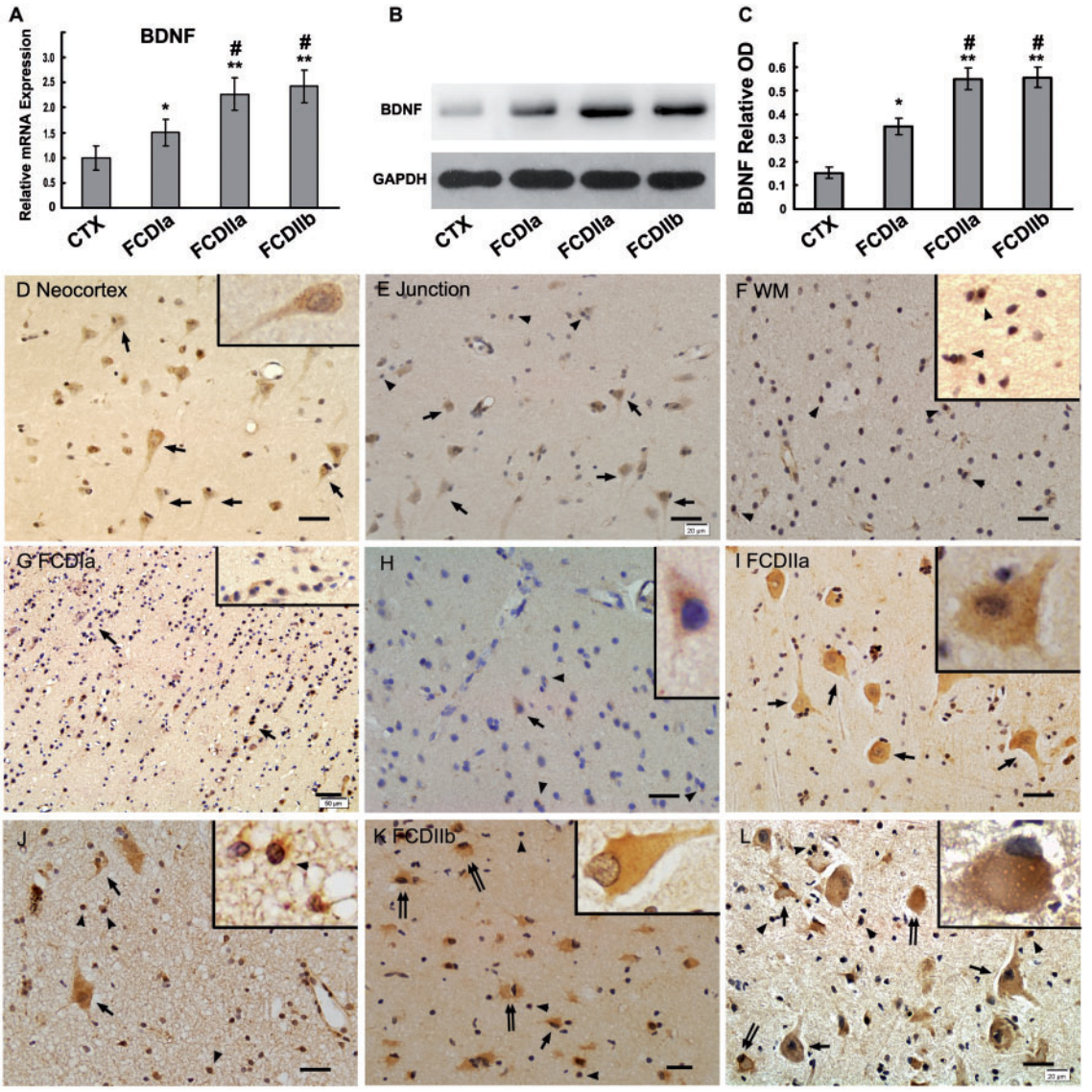

FIGURE 5. Expression of BDNF in FCD types Ia, IIa, IIb and normal CTX specimens. **(A)** Real-time polymerase chain reaction analysis of BDNF mRNA expression in CTX, FCDIa, FCDIIa, and FCDIIb ($n = 10$ in each group). Greater BDNF mRNA levels were observed in the FCDIa, FCDIIa, and FCDIIb samples versus the CTX samples. BDNF mRNA expression was significantly greater in the FCDIIa and FCDIIb cortical lesions versus the FCDIa specimens. Error bars represent SE; *$p < 0.05$; **$p < 0.01$ versus CTX; #$p < 0.05$ versus FCDIa; ANOVA. **(B)** Representative immunoblots of BDNF in total homogenates from the FCDIa, FCDIIa, FCDIIb, and CTX samples. **(C)** Densitometric analyses of the Western blots. There was a significant increase in BDNF protein levels in the total homogenates from the FCDIa, FCDIIa, FCDIIb samples ($n = 10$ in each series) versus the CTX samples ($n = 10$). The expression of BDNF protein was also significantly greater in the FCDIIa and FCDIIb cortical lesions versus the FCDIa specimens. Error bars represent SE; *$p < 0.05$, **$p < 0.01$ versus CTX, #$p < 0.05$ versus FCDIa; ANOVA. There was no significant difference BDNF expression levels between the FCDIIa and FCDIIb samples. **(D–L)** BDNF-immunoreactivity (-IR) in the CTX, FCDIa, FCDIIa, and FCDIIb samples. Representative immunohistochemical staining for BDNF in the control cortex **(D)**, junction **(E),** and white matter **(F)** showing weak to moderate BDNF staining in neurons (arrows in **D** and **E**) and glia-like cells (arrowheads in **E** and **F**). In FCDI samples there is moderate to strong BDNF staining in neurons (arrows in **G** and **H**), including the microcolumns (insert in **G**) in the gray matter and heterotopic neurons (arrows in **H**) in the white matter. There was also moderate BDNF staining in glia-like cells (arrowheads in **H**). There is moderate to strong BDNF staining in FCDIIa samples in the DNs (arrows in **I** and **J**) and glia-like cells (arrowheads in **J** and insert in **J**). In FCDIIb samples there was moderate to strong BDNF-IR in the DNs (arrows in **K, L** and insert in **K**) and BCs (double-arrows in **K, L** and insert in **L**), along with moderate to strong staining in glia-like cells (arrowheads in **K** and **L**). Scale bars: **D–F, H–J, L** = 30 μm; **G, K** = 50 μm.

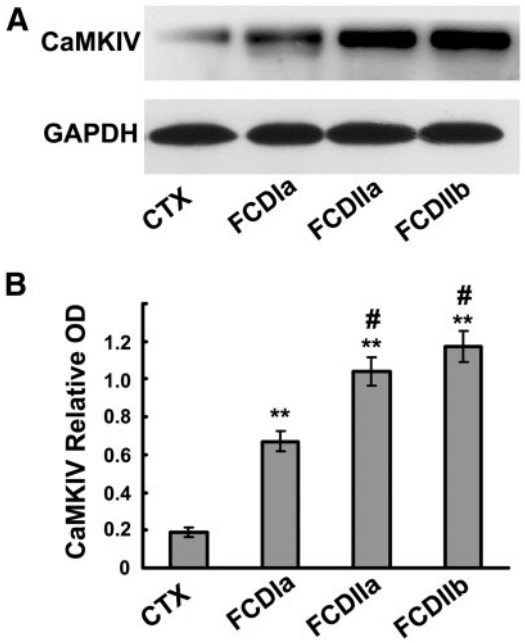

FIGURE 6. Expression of CaMKIV protein in normal CTX and FCD types Ia, IIa, and IIb. **(A)** Representative immunoblots of CaMKIV in total homogenates from FCD types Ia (FCDIa), IIa (FCDIIa), and IIb (FCDIIb) lesions and CTX samples tissues ($n = 10$ in each group). **(B)** Densitometric analyses of the Western blots. There were significantly greater CaMKIV protein levels in the FCDIa, FCDIIa, and FCDIIb tissues versus the control samples. Importantly, protein levels of CaMKIV were significantly greater in the FCDIIa and FCDIIb cortical lesions versus FCDIa specimens. Error bars represent SE; $^*p < 0.05$, $^{**}p < 0.01$ versus CTX; $\#p < 0.05$ versus FCDIa; ANOVA.

activation of PLC-γ and the production of DAG and IP_3. DAG directly activates TRPC3 and TRPC6, leading to neuronal survival (39). Therefore, we speculate that BDNF/TRPC signaling may support or enhance the survival of immature cells (DNs and BCs) that interact with cells that have reached maturity and have normal synaptic connections to produce seizures (40).

In this study, we demonstrated increases in TRPC6 and CaMKIV expression in FCD patients compared with controls. The establishment of dendritic morphology is critical for the development of neuronal circuits (41). Dendrites are the primary sites of synaptic connections from the input neurons as well as the site of synaptic output communication to other neurons. TRPC6 is highly expressed during the period of maximal dendritic growth and promotes dendritic growth through a CaMKIV-CREB-dependent pathway (14, 42). TRPC3 and TRPC6 were also shown to participate in diverse mechanisms of synaptic reorganization in the mossy fiber pathway in temporal lobe epilepsy (43). We also found that most of the TRPC6-positive neurons in FCD patients, particularly the neuronal microcolumns, heterotopic neurons, DNs, and BCs, colabeled with glutamate. Furthermore, TRPC6 was mainly localized to excitatory postsynaptic sites and was important for the development of dendritic spines and excitatory synapses *in vitro* and *in vivo* (15). Therefore, we propose that the highly expressed TRPC6 in FCD patients promotes dendritic growth and the development of dendritic spines and excitatory synapses via the CaMKIV-CREB pathway, resulting in dendritic abnormalities and abnormally excitable circuits.

In conclusion, this study is the first to report increased expression of TRPC6 in FCD patient tissues; TRPC6 was mainly distributed in the heterotopic neurons, DNs, and BCs. BDNF was upregulated in neurons and glia-like cells in FCD patients, particularly the heterotopic neurons, DNs, and BCs. The migration of DNs and BCs may be mediated by BDNF through guiding the nerve growth cone via TRPC6. BDNF/TRPC6 signaling may support or enhance the survival of DNs and BCs and promote dendritic growth through the CaMKIV-CREB pathway, resulting in abnormal synaptic connections between immature and mature cells, which can facilitate and potentially initiate seizure activity. Considering our findings together, it is clear why the expression levels of BDNF, TRPC6, and CaMKIV were higher in FCDIIa and FCDIIb patients than in FCDIa patients. Because heterotopic neurons, DNs, and BCs are characteristic of FCD and play a significant role in the abnormally excitable circuit, these results suggest that the overexpression of BDNF and TRPC6 and the activation of the TRPC6 signal transduction pathway in FCD lesions may contribute to the pathogenesis and epileptogenesis of FCD.

ACKNOWLEDGMENTS

The authors express their sincere thanks to Ms. Wei Sun and Ms. Jin Peng (senior experimental division and assistant laboratory technician, respectively; Central Laboratory, Third Military Medical University, Chongqing, China) for their assistance with the confocal laser scanning microscopy images. We would also like to thank Dr Ning An and Dr Zhi Hou (neurosurgeons; Department of Neurosurgery, Xin'qiao Hospital, Third Military Medical University, Chongqin, China) for their assistance in collecting the FCD specimens.

REFERENCES

1. Palmini A, Holthausen H. Focal malformations of cortical development: A most relevant etiology of epilepsy in children. Handb Clin Neurol 2013;111:549–65
2. Schwartzkroin PA, Walsh CA. Cortical malformations and epilepsy. Ment Retard Dev Disabil Res Rev 2000;6:268–80
3. Crino PB, Miyata H, Vinters HV. Neurodevelopmental disorders as a cause of seizures: Neuropathologic, genetic, and mechanistic considerations. Brain Pathol 2002;12:212–33
4. Mischel PS, Nguyen LP, Vinters HV. Cerebral cortical dysplasia associated with pediatric epilepsy. Review of neuropathologic features and proposal for a grading system. J Neuropathol Exp Neurol 1995;54:137–53
5. Crino PB, Eberwine J. Cellular and molecular basis of cerebral dysgenesis. J Neurosci Res 1997;50:907–16
6. Cotter DR, Honavar M, Everall I. Focal cortical dysplasia: A neuropathological and developmental perspective. Epilepsy Res 1999;36:155–64
7. Najm IM, Tilelli CQ, Oghlakian R. Pathophysiological mechanisms of focal cortical dysplasia: A critical review of human tissue studies and animal models. Epilepsia 2007;48(Suppl 2):21–32
8. Mathern GW, Andres M, Salamon N, et al. A hypothesis regarding the pathogenesis and epileptogenesis of pediatric cortical dysplasia and hemimegalencephaly based on MRI cerebral volumes and NeuN cortical cell densities. Epilepsia 2007;48(Suppl 5):74–8

9. Lamparello P, Baybis M, Pollard J, et al. Developmental lineage of cell types in cortical dysplasia with balloon cells. Brain 2007;130:2267–76
10. Shu HF, Kuang YQ, Liu SY, et al. Endogenous subventricular zone neural progenitors contribute to the formation and hyperexcitability of experimental model of focal microgyria. J Mol Neurosci 2014;52: 586–97
11. Vazquez G, Wedel BJ, Aziz O, et al. The mammalian TRPC cation channels. Biochim Biophys Acta 2004;1742:21–36
12. Bon RS, Beech DJ. In pursuit of small molecule chemistry for calcium-permeable non-selective TRPC channels—Mirage or pot of gold? Br J Pharmacol 2013;170:459–74
13. Vannier B, Peyton M, Boulay G, et al. Mouse trp2, the homologue of the human trpc2 pseudogene, encodes mTrp2, a store depletion-activated capacitative Ca2+ entry channel. Proc Natl Acad Sci U S A 1999;96: 2060–4
14. Tai Y, Feng S, Ge R, et al. TRPC6 channels promote dendritic growth via the CaMKIV-CREB pathway. J Cell Sci 2008;121:2301–7
15. Zhou J, Du W, Zhou K, et al. Critical role of TRPC6 channels in the formation of excitatory synapses. Nat Neurosci 2008;11:741–3
16. Li Y, Jia YC, Cui K, et al. Essential role of TRPC channels in the guidance of nerve growth cones by brain-derived neurotrophic factor. Nature 2005;434:894–8
17. Redmond L, Ghosh A. Regulation of dendritic development by calcium signaling. Cell Calcium 2005;37:411–6
18. Blumcke I, Thom M, Aronica E, et al. The clinicopathologic spectrum of focal cortical dysplasias: A consensus classification proposed by an ad hoc task force of the ILAE diagnostic methods commission. Epilepsia 2011;52:158–74
19. Guo W, Zheng DH, Sun FJ, et al. Expression and cellular distribution of the interleukin 2 signaling system in cortical lesions from patients with focal cortical dysplasia. J Neuropathol Exp Neurol 2014;73:206–22
20. Saper CB. An open letter to our readers on the use of antibodies. J Comp Neurol 2005;493:477–8
21. Saper CB, Sawchenko PE. Magic peptides, magic antibodies: Guidelines for appropriate controls for immunohistochemistry. J Comp Neurol 2003;465:161–3
22. Minke B. TRP channels and Ca2+ signaling. Cell Calcium 2006;40: 261–75
23. Sun FJ, Guo W, Zheng DH, et al. Increased expression of TRPV1 in the cortex and hippocampus from patients with mesial temporal lobe epilepsy. J Mol Neurosci 2013;49:182–93
24. Shu HF, Yu SX, Zhang CQ, et al. Expression of TRPV1 in cortical lesions from patients with tuberous sclerosis complex and focal cortical dysplasia type IIb. Brain Dev 2013;35:252–60
25. Tai C, Hines DJ, Choi HB, et al. Plasma membrane insertion of TRPC5 channels contributes to the cholinergic plateau potential in hippocampal CA1 pyramidal neurons. Hippocampus 2011;21:958–67
26. Phelan KD, Shwe UT, Abramowitz J, et al. Critical role of canonical transient receptor potential channel 7 in initiation of seizures. Proc Natl Acad Sci USA 2014;111:11533–8
27. Kunert-Keil C, Bisping F, Kruger J, et al. Tissue-specific expression of TRP channel genes in the mouse and its variation in three different mouse strains. BMC Genomics 2006;7:159
28. Sherwood CC, Raghanti MA, Stimpson CD, et al. Inhibitory interneurons of the human prefrontal cortex display conserved evolution of the phenotype and related genes. Proc Biol Sci 2010;277:1011–20
29. Benavides-Piccione R, DeFelipe J. Distribution of neurons expressing tyrosine hydroxylase in the human cerebral cortex. J Anat 2007;211:212–22
30. Arai A, Saito T, Hanai S, et al. Abnormal maturation and differentiation of neocortical neurons in epileptogenic cortical malformation: Unique distribution of layer-specific marker cells of focal cortical dysplasia and hemimegalencephaly. Brain Res 2012;1470:89–97
31. Dent EW, Gertler FB. Cytoskeletal dynamics and transport in growth cone motility and axon guidance. Neuron 2003;40:209–27
32. Shim S, Goh EL, Ge S, et al. XTRPC1-dependent chemotropic guidance of neuronal growth cones. Nat Neurosci 2005;8:730–5
33. Cepeda C, Andre VM, Levine MS, et al. Epileptogenesis in pediatric cortical dysplasia: The dysmature cerebral developmental hypothesis. Epilepsy Behav 2006;9:219–35
34. Chen A, Xiong LJ, Tong Y, et al. The neuroprotective roles of BDNF in hypoxic ischemic brain injury. Biomed Rep 2013;1:167–76
35. Lu B, Nagappan G, Lu Y. BDNF and synaptic plasticity, cognitive function, and dysfunction. Handb Exp Pharmacol 2014;220:223–50
36. Phillips K, Keane K, Wolfe BE. Peripheral brain derived neurotrophic factor (BDNF) in bulimia nervosa: A systematic review. Arch Psychiatr Nurs 2014;28:108–13
37. Niu C, Yip HK. Neuroprotective signaling mechanisms of telomerase are regulated by brain-derived neurotrophic factor in rat spinal cord motor neurons. J Neuropathol Exp Neurol 2011;70:634–52
38. Ghosh A, Carnahan J, Greenberg ME. Requirement for BDNF in activity-dependent survival of cortical neurons. Science 1994;263: 1618–23
39. Jia Y, Zhou J, Tai Y, et al. TRPC channels promote cerebellar granule neuron survival. Nat Neurosci 2007;10:559–67
40. Cepeda C, Andre VM, Vinters HV, et al. Are cytomegalic neurons and balloon cells generators of epileptic activity in pediatric cortical dysplasia? Epilepsia 2005;46(Suppl 5):82–8
41. Cline HT. Dendritic arbor development and synaptogenesis. Curr Opin Neurobiol 2001;11:118–26
42. Goel M, Sinkins WG, Schilling WP. Selective association of TRPC channel subunits in rat brain synaptosomes. J Biol Chem 2002;277:48303–10
43. Zeng C, Zhou P, Jiang T, et al. Upregulation and diverse roles of TRPC3 and TRPC6 in synaptic reorganization of the mossy fiber pathway in temporal lobe epilepsy. Mol Neurobiol 2015;52:562–72